



Cite this: *RSC Adv.*, 2018, 8, 21340

Investigation of the reaction pathway for synthesizing methyl mercaptan (CH₃SH) from H₂S-containing syngas over K–Mo-type materials†

Jichang Lu,^a Pan Liu,^a Zhizhi Xu,^a Sufang He^{*b} and Yongming Luo ^{*a}

The reaction pathway for synthesizing methyl mercaptan (CH₃SH) using H₂S-containing syngas (CO/H₂S/H₂) as the reactant gas over SBA-15 supported K–Mo-based catalysts prepared by different impregnation sequences was investigated. The issue of the route to produce CH₃SH from CO/H₂S/H₂ has been debated for a long time. In light of designed kinetic experiments together with thermodynamics analyses, the corresponding reaction pathways in synthesizing CH₃SH over K–Mo/SBA-15 were proposed. In the reaction system of CO/H₂S/H₂, COS was demonstrated to be generated firstly *via* the reaction between CO and H₂S, and then CH₃SH was formed *via* two reaction pathways, which were both the hydrogenation of COS and CS₂. The resulting CH₃SH was in a state of equilibrium of generation and decomposition. Decomposition of CH₃SH was found to occur *via* two reaction pathways; one was that CH₃SH first transformed into two intermediates, CH₃SCH₃ and CH₃SSCH₃, which were then further decomposed into CH₄ and H₂S; another was the direct decomposition of CH₃SH into C, H₂S and H₂. Moreover, the catalyst (K–Mo/SBA-15) prepared with co-impregnation exhibits higher catalytic activities than the catalysts (K/Mo/SBA-15 and Mo/K/SBA-15) prepared by the sequence of impregnation. Based on characterization of the oxidized, sulfided and spent catalysts *via* N₂ adsorption–desorption isotherms, XRD, Raman, XPS and TPR, it was found that two K-containing species, K₂Mo₂O₇ and K₂MoO₄, were oxide precursors, which were then converted into main K-containing MoS₂ species. The CO conversion was closely related to the amount of edge reactive sulfur species that formed the sulfur vacancies over MoS₂ phases.

Received 21st April 2018
 Accepted 4th June 2018

DOI: 10.1039/c8ra03430c

rsc.li/rsc-advances

Introduction

The exorbitant emissions of reduced sulfur species (H₂S, COS and CS₂) together with carbon-containing compound CO from reduced industrial flue gases into the atmosphere would be potentially responsible for the increasingly serious environment pollution (haze and acid rain), which is threatening human survival and health in most developing countries. At present, most methods for utilizing sulfur and carbon species from reduced industrial flue gases are independent.^{1,2} This indicates that the reduced sulfur species are firstly removed *via* various methods.^{3,4} Then, the purified carbon species would be used to produce chemical products (such as alcohols).^{5,6} Herein, a feasible route to synergistically utilize hydrogen sulfide (H₂S)

together with syngas (CO/H₂) for synthesizing a high value-added product, methanethiol (CH₃SH), is promising (eqn (1)).^{7,8} CH₃SH is one of the urgently important chemical intermediates for producing organic sulfur compounds in poultry feed, medicine, pesticides and so on,^{9,10} and large scale production of methanethiol is generally based on the thiolation of H₂S with methanol (CH₃OH) from syngas.^{11,12} This one-step conversion of the industry gas contained sulfur species to CH₃SH not only decreases the consumption of clean fuel (CH₃OH)¹³ but also could co-recycle acid gas (H₂S) and the low-cost and wide-range sources of synthesis gas (CO/H₂), which exhibits the increasingly favorable economies and has attracted considerable attentions in the industrial applications.^{14,15}



In general, alkali-promoted molybdenum (Mo) or tungsten (W) based materials have been widely used as the effective active catalysts for synthesizing CH₃SH^{9,16,17} and alumina (Al₂O₃) and silicon dioxide (SiO₂) were selected as the supports for loading and dispersing these Mo (or W) containing active phases.^{15,18,19} However, the low catalytic activity and selectivity are obtained for these alkali-promoted Mo (or W) based catalysts, which leads to

^aFaculty of Environmental Science and Engineering, Kunming University of Science and Technology, Kunming 650500, P. R. China. E-mail: environcatalysis222@yahoo.com; Fax: +86-871-65103845; Tel: +86-871-65103845

^bResearch Center for Analysis and Measurement, Kunming University of Science and Technology, Kunming 650093, P. R. China. E-mail: shuca1983@163.com; Fax: +86 871 65111617; Tel: +86 871 65119674

† Electronic supplementary information (ESI) available. See DOI: 10.1039/c8ra03430c



the hardly realization of harmlessness and resource utilization. In general, two significant factors are still in a controversial state, *i.e.*, the presence of complex reaction network as well as the uncertain reactive phases, which makes it difficult to further improve the catalytic activity. The comprehensive of reactive active phases will be given in the future. Therefore, this work is focus on the investigation of the reaction pathway.

The well understanding of reaction network would provide essential insight into the comprehending of reaction mechanism, and could further promote the catalytic performances. Several reaction networks have been proposed by different groups over the K–Mo (K–W) based catalysts. Employing mixtures (CO/H₂S/H₂) as reaction system to synthesize CH₃SH can be traced back to 1960s by Olin *et al.*⁸ who found that the overall reaction process was followed by eqn (1). Afterwards, Barrault and Yang's^{16,19} pointed out that CO molecule was firstly reacted with H₂S to form COS, and then the hydrogenation of COS generated CH₃SH and H₂O. This reaction pathway has been considered as the mainstream reaction for a long time, while some matters such as H₂O are not detected, making it difficult to confirm the reaction network. Other research groups^{20,21} reported that, based on the detected new matter of thiophene, the modified Fischer–Tropsch process followed by a surface polymerisation mechanism was deemed to be an alternative reaction pathway. Recently, Lercher and coworker^{22,23} investigated the synthesis of CH₃SH using COS/H₂/H₂S as reactants over sulfide K₂MoO₄/SiO₂, and several skillful activity tests were performed to evaluate the reaction pathway. They considered that COS could decompose rapidly to CO and H₂S, meanwhile, COS disproportionated to CO₂ and CS₂, then CS₂, the reaction intermediate, was hydrogenated to CH₃SH. In a word, the debate about the reaction pathway for synthesizing CH₃SH has been continued because of the existence of a dozen reactions in this system. Therefore, it is challenging to completely understand the reaction network for converting CO/H₂/H₂S to CH₃SH. Moreover, thermodynamic is a significant criterion for the degree of a chemical reaction to take place. A typical software of HSC Chemistry was usually applied to calculate the thermodynamic parameters to evaluate whether a reaction will occur, including enthalpy change, Gibbs free energy changes and equilibrium constant. However, since all the basic parameter about CH₃SH is missing in the Database of HSC Chemistry software, the requirement for thermodynamic parameters of reactions containing CH₃SH is urgent.

With a review of previous works, further studies on the reaction network for synthesizing CH₃SH from CO/H₂/H₂S are still necessary to provide further documents. In our previous work, SBA-15 was used as a new silica based support due to its significant improvement in catalytic activity, selectivity and durability,^{24,25} and alkali metal K was selected to be one of the best additives.²⁶ Thus, SBA-15 supported K–Mo based catalysts were prepared *via* different impregnation sequence to obtain the results of catalytic activity and to figure out the reaction pathway. Moreover, several designed experiments with different gas components were performed. The corresponding reaction routes were proposed, and the thermodynamic parameters were calculated to confirm the feasibility of the synthetic reactions.

Experimental selection

Catalysts preparation

SBA-15 was prepared by using nonionic triblock copolymer EO₂₀-PO₇₀-EO₂₀ (Pluronic P123) and tetraethyl silicate TEOS as the structure-directing agent and silicon source, respectively, in according with our previous literatures.^{27,28} K–Mo/SBA-15 catalyst was prepared by SBA-15, (NH₄)₆Mo₇O₂₄·6H₂O and K₂CO₃ *via* the incipient-wetness co-impregnation method, and the loading of Mo (based on MoO₃) and molar ratios of K/Mo were 25 wt% and 2/1, respectively. After impregnation, the sample was dried at 120 °C for 24 h and subsequently calcined at 400 °C for 3 h in the air. K/Mo/SBA-15 and Mo/K/SBA-15 were carried out by a sequential impregnation. In a typical procedure, Mo/SBA-15 or K/SBA-15 was firstly prepared by incipient-wetness impregnation with (NH₄)₆Mo₇O₂₄·6H₂O and K₂CO₃, respectively. Subsequently, calcined Mo/SBA-15 and K/SBA-15 were further used to synthesize K/Mo/SBA-15 or Mo/K/SBA-15 catalysts by incipient-wetness impregnation with K₂CO₃ and (NH₄)₆Mo₇O₂₄·6H₂O, respectively. Finally, the obtained samples were pretreated as the procedure mentioned before. All the catalysts were denoted as oxidized samples.

Catalysts characterization

N₂ adsorption–desorption isotherms were conducted on a Beckman Coulter's SA3100 automatic analyzer at –196 °C. BET surface area of the samples was performed by using BET method according to the data of adsorption branch, and the pore size distribution was calculated by the BJH method by using the desorption branch data. X-ray diffraction (XRD) patterns were recorded on a Japanese Rigaku's D/Max-1200 diffractometer using Cu K α -radiation ($\lambda = 0.154056$ nm) at 40 kV and 30 mA. The evaluation of the diffractogram was made by MDI Jade 5.0 software to identify the crystalline phases within the catalysts. Raman spectrum was recorded by using a Via Reflex Raman spectrometer with 514 nm emission line from Ar⁺ laser at room temperature. X-ray photoelectron spectroscopy (XPS) technique was employed to determine the composition and chemical state of different elements using a PHI 5000 VersaProbe II with non-monochromatic Al K α radiation (1486.6 eV). CasaXPS software was used to fit the corresponding spectra, and the charge referencing was detected against adventitious carbon with the C 1s at 284.6 eV. Temperature programmed reduction of hydrogen (H₂-TPR) was conducted on the apparatus equipped with a TCD detector to measure the reactive surface sulfur species over sulfided MoS₂ materials. Prior to H₂-TPR measurement, 50 mg of sulfided samples were pretreated with the flow of Argon (Ar, 30 ml min⁻¹) at 673 K for 1 h and then were cooled down to 373 K. Subsequently, a mixture of 10 vol% H₂/Ar (30 ml min⁻¹) was introduced and the pretreated samples were heated at a rate of 10 K min⁻¹ to 1173 K.

Catalytic activity test

The catalytic activity experiments were carried out in a 6 mm i.d. quartz fixed-bed reactor. 0.4 g catalyst (40–60 mesh) mixed with quartz grains was secured with quartz wool in the isothermal region of the reactor. Then, the reactant gas (CO/H₂S/H₂ = 1 : 5 : 4)



was introduced into the reactor under the conditions of $P = 0.2$ MPa, $GHSV = 1000$ h⁻¹ with different reaction temperature (523–673 K). Prior to each activity evaluation measurements, all the samples were presulfided in the gas stream with $CO/H_2S/H_2 = 1 : 5 : 4$ (30 ml min⁻¹) at 553 K for 6 h. Those catalysts are denoted as sulfided samples. After the catalytic activity test, all the catalysts were denoted as spent samples. Reaction products were online detected using three GC fitted with one flame ionization detector (FID), two flame photometric detectors (FPD) and two thermal conductivity detectors (TCD). Carbon hydrogen components including CH_3SH , CH_4 , little C_2H_4 and C_2H_6 were detected by FID with a porapak Q column. Two FPD equipping with the same HP-Plot/Q capillary column and two different volume of six-way valve were employed to detect different concentration (0.1 ppm to 150000 ppm) of sulfur-containing matters including COS, CS_2 , CH_3SH and H_2S . TCDs equipped with TDX-01 carbon molecular sieve and porapak Q column were used to detect H_2 , CO, CO_2 and H_2O . The CO conversion and products selectivity were calculated by the following equation:

$$\text{con. CO} = \frac{(C_{CO,in} - C_{CO,out})}{C_{CO,in}} \times 100\%$$

where $C_{CO,in}$ and $C_{CO,out}$ correspond to the inlet and outlet concentrations of CO (ppm), respectively.

The selectivity of products was calculated according to the balance of carbon, in which the main carbon-containing products, CH_3SH , COS, CO_2 , CH_4 , are included.

$$\begin{aligned} \text{sel.}_X &= \frac{X_i}{\sum_{i=1}^n X_i} \times 100\% \\ &= \frac{C_i}{C(CH_3SH) + C(COS) + C(CO_2) + C(CH_4)} \times 100\% \end{aligned}$$

where C_i is the concentration of products (ppm).

Reaction pathway research

To better figure out the reaction pathway, six experiments inducing different reactant gas were designed, and the experiment conditions were listed as follows. Then, the reactant gas was separately introduced into the reactor under the same conditions of $P = 0.2$ MPa, $GHSV = 1000$ h⁻¹ with different reaction temperature (523–673 K).

- (1) The reactant gas: $CO_2 : H_2S : N_2 = 1 : 1 : 8$ (30 ml min⁻¹).
- (2) The reactant gas: $CO_2 : H_2 : N_2 = 1 : 1 : 8$ (30 ml min⁻¹).
- (3) The reactant gas: $CO_2 : H_2 : CO : N_2 = 1 : 1 : 1 : 7$ (30 ml min⁻¹).
- (4) The reactant gas: $CO/H_2 = 1 : 4$ (30 ml min⁻¹);
- (5) The reactant gas: $CO/H_2S = 1 : 5$ (30 ml min⁻¹);
- (6) The reactant gas: 1% CH_3SH (30 ml min⁻¹).

Results and discussion

Effect of impregnation sequence

CO conversions of Mo/K/SBA-15, K/Mo/SBA-15 and K-Mo/SBA-15 are presented in Fig. 1(A). The highest CO conversion is

observed for K-Mo/SBA-15. The CO conversion first increases and then decreases with the temperature increasing, which reaches the maximal conversion (42.67%) at 598 K. Mo/K/SBA-15 exhibits the lowest CO conversion, whereas the CO conversion of K/Mo/SBA-15 is intermediate between K-Mo/SBA-15 and Mo/K/SBA-15. The CO conversion of those two catalysts is increasing with the temperature rising while the CO conversion is not more than 30% in the end (673 K). The selectivities of COS, CH_3SH , CO_2 and CH_4 over Mo/K/SBA-15, K/Mo/SBA-15 and K-Mo/SBA-15 are presented in Fig. 1(B–E). The selectivity of COS over the three catalysts (shown in Fig. 1B) is dropping with the temperature rising. The COS selectivity of Mo/K/SBA-15 is remarkably higher than other two catalysts when the temperature is lower than 593 K, while the varied trend of COS selectivity for these three catalysts are roughly similar. Moreover, the CH_3SH selectivity of K-Mo/SBA-15 is obviously higher than that of Mo/K/SBA-15 and K/Mo/SBA-15 when the temperature is below 623 K. As for the selectivity of CO_2 (shown in Fig. 1D), it is relatively stable in the temperature range in addition to that at 523 K. The selectivity of CH_4 (shown in Fig. 1E) has been going up with the increasing reaction temperature, the relatively higher CH_4 selectivity is obtained on K/Mo/SBA-15 instead of Mo/K/SBA-15 and K-Mo/SBA-15. Considered the CO conversion and CH_3SH selectivity, K-Mo/SBA-15 prepared by incipient-wetness co-impregnation method exhibits the higher catalytic performances than those of K/Mo/SBA-15 and Mo/K/SBA-15 samples prepared by a sequential impregnation method.

Characterization of active species

The textural parameters of SBA-15, Mo/K/SBA-15, K/Mo/SBA-15, K-Mo/SBA-15 are summarized in Table 1. SBA-15 exhibits the type IV isotherms with H1-type hysteresis loops attributed to typical mesoporous structure (not shown).²⁹ After the incorporation of K and Mo oxide precursor, all the BET surface area, pore volume and pore size of three samples decreases to some degree. Compared to K/Mo/SBA-15, BET surface area, pore volume and pore size of Mo/K/SBA-15 and K-Mo/SBA-15 significantly decrease, indicating the interaction of alkaline K species with silica-based SBA-15 support leading the destroy of the mesoporous structure. K/Mo/SBA-15, K-Mo/SBA-15 samples shows the BET surface area of 143.9 and 68.1 m² g⁻¹. Considering the opposite activity results (K/Mo/SBA-15 < K-Mo/SBA-15), we can deduce that there is possibly no direct relationship between catalysts activity and BET surface area.

The crystalline phases of oxidized, sulfided and spent catalysts are characterized by X-ray diffraction (XRD), and the corresponding XRD patterns were presented in Fig. 2. All the oxidized Mo/K/SBA-15, K/Mo/SBA-15, K-Mo/SBA-15 samples show the same X-ray diffraction lines, indicating the formation of the same structures of oxide precursors. The dominant diffraction peaks shown in the oxidized samples are assigned to $K_2Mo_2O_7$ (JCPDS-ICDD no. 36-0347) and K_2MoO_4 (JCPDS-ICDD no. 01-0766). Small MoO_3 species (JCPDS-ICDD no. 05-0508) is also detected for oxidized catalysts. After sulfided at 553 K, K_2SO_4 phase (JCPDS-ICDD no. 05-0613) is observed for K-Mo/SBA-15 and K/Mo/SBA-15, and $K_2S_2O_8$ phase (JCPDS-ICDD



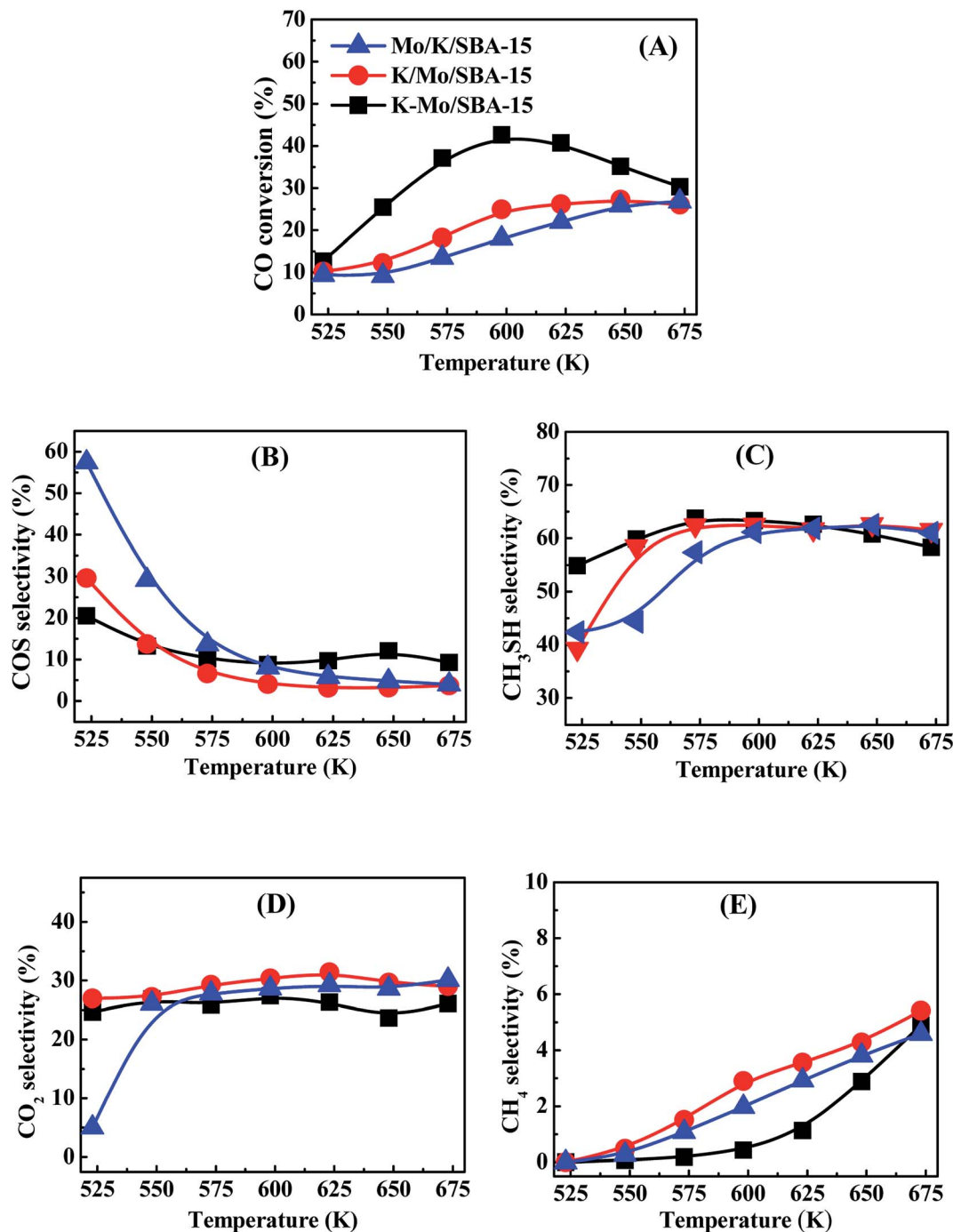


Fig. 1 CO conversion (A) and products selectivity COS (B), CH₃SH (C), CO₂(D) and CH₄ (E) of Mo/K/SBA-15 (blue light triangle), K/Mo/SBA-15 (red light circle) and K-Mo/SBA-15 (back light square). Reaction conditions: 0.2 MPa, 1000 h⁻¹ and CO/H₂S/H₂ = 1 : 5 : 4.

no.32-0846) is detected for K/Mo/SBA-15 and Mo/K/SBA-15. Those sulfate and persulfate species are probably originated from the conversion of intermediate K₂S with water readily and irreversibly in the transfer process, leading finally to the agglomerated K₂SO₄ and K₂S₂O₈ phases.²² The difference in the formed sulfate species over three catalysts may be due to the distinguished interaction among K oxide, Mo oxide and SBA-15 in the process of different impregnation sequence. In the spent K-Mo/SBA-15 sample, the K₂SO₄ phase disappears, and K₂S₂O₈

(JCPDS-ICDD no.32-0846) phase is also formed during the reaction. It is known that the sulfate phases is an undesired species and is inactive for catalytic reaction, which could give rise to the decrease in the catalytic performance at high temperature to some degree. Moreover, it should be noted that the peaks at 14.5°, 33.2°, 58.8° attributed to MoS₂ (JCPDS-ICDD no. 024-0513) are not distinct, and the intensity of MoS₂ found in the sulfided catalyst is pretty low. It is speculated that MoS₂ phase exists on the catalysts in the form of amorphous state or



Table 1 Textural characteristics of Mo/K/SBA-15, K/Mo/SBA-15 and K-Mo/SBA-15

Samples	S_{BET}^a ($\text{m}^2 \text{g}^{-1}$)	V_p^b ($\text{cm}^3 \text{g}^{-1}$)	D_p^c (nm)
SBA-15	1022.4	1.11	4.9
Mo/K/SBA-15	36.8	0.07	3.8
K/Mo/SBA-15	143.9	0.24	6.4
K-Mo/SBA-15	68.1	0.14	3.8

^a S_{BET} , BET surface area. ^b V_p , pore volume. ^c D_p , average pore diameter.

the size and amount of MoS_2 species is lower than that of XRD detection limit under the sulfured progress with 553 K. After reaction, MoS_2 (JCPDS-ICDD no. 024-0513) diffraction peak is obviously observed and becomes the main crystalline phase, indicating the crystalline MoS_2 phase with higher size is formed between 553 K to 673 K.

Raman spectra of oxidized, sulfided and spent catalysts are shown in Fig. 3A and B, respectively, to characterize the active species. For the oxidized samples, the bands at 849 and 711 cm^{-1} are attributed to the presence of $\text{K}_2\text{Mo}_2\text{O}_7$ (ref. 30) and other bands are assigned to K_2MoO_4 species, in agreement with

XRD. For sulfided and spent samples, three main lines at 382, 408, and 450 cm^{-1} can be observed in all the spectrum. The band at 382 cm^{-1} corresponds to the Mo-S stretching mode along the basal plane, while the one at 408 cm^{-1} is attributed to a S-Mo-S stretching mode along to the C-axis, and the band at 450 cm^{-1} is assigned to the second-order scattering.³¹ Those weak Raman peaks suggests MoS_2 species is presented in the form of amorphous state in the sulfided catalysts. The spectra of spent catalysts is very similar with that of sulfided sample, however, there is significant difference in the peak intensity between sulfided and spent samples, indicating that partial oxidized K-Mo precursors are further converted into MoS_2 species during reaction process.

To further investigate the phase transformation in the catalysis progress, the sulfided and spent catalysts of three catalysts are characterized by XPS. The decomposition constraints about Mo 3d are referred to Cordova *et al.*³² and Qiu *et al.*³³ Fig. 4 exhibits the decomposition of the Mo 3d spectra of sulfided and spent Mo/K/SBA-15, K/Mo/SBA-15 and K-Mo/SBA-15 samples. For the sulfided catalysts, the components at 229.2, 230.7 and 233.1 eV are attributed to Mo 3d_{5/2} components

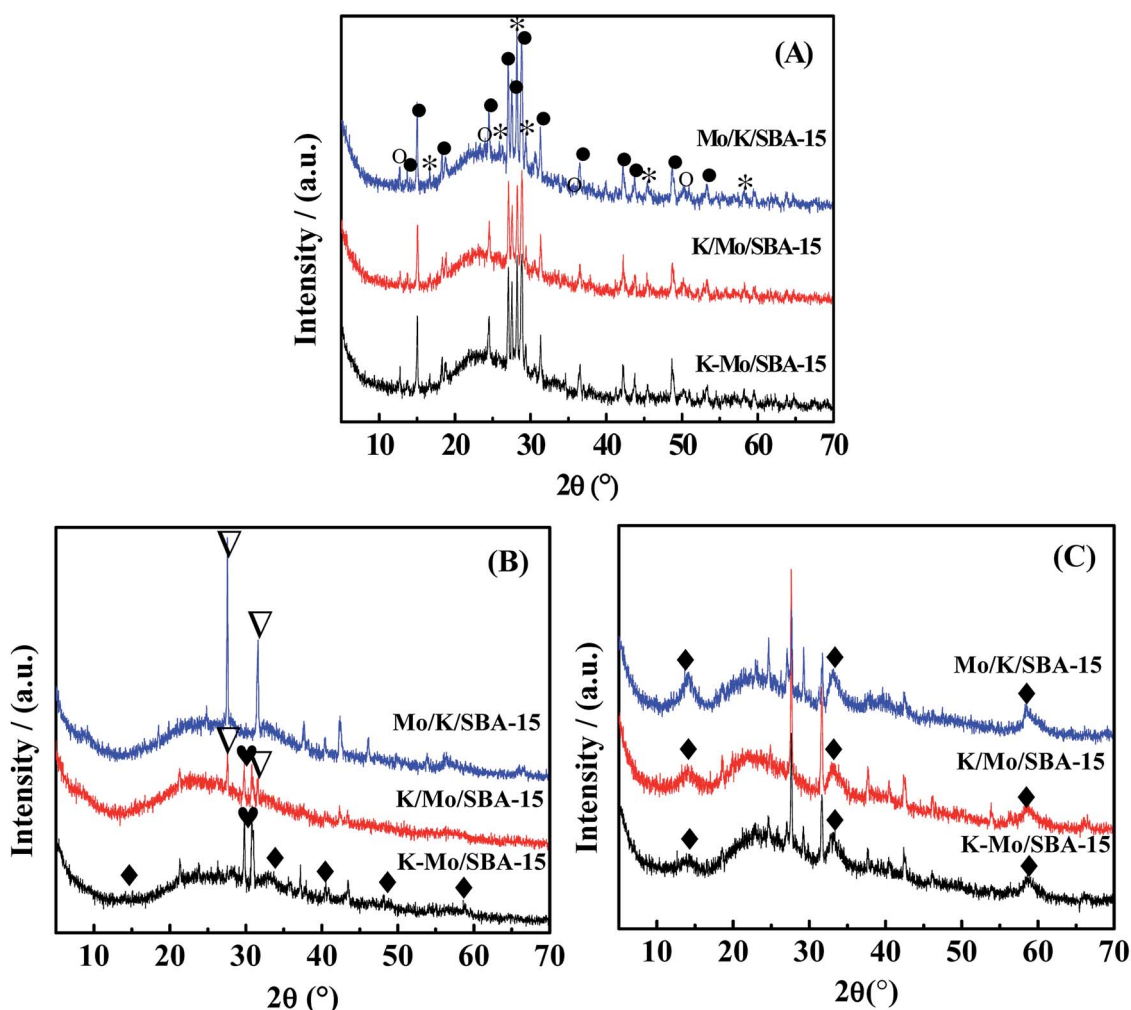


Fig. 2 XRD diffractograms of (A) oxide precursors of catalysts, (B) sulfided catalysts and (C) spent catalysts. MoO_3 (○), MoS_2 (◆), $\text{K}_2\text{Mo}_2\text{O}_7$ (●), K_2MoO_4 (*), K_2SO_4 (♥), $\text{K}_2\text{S}_2\text{O}_8$ (▽).



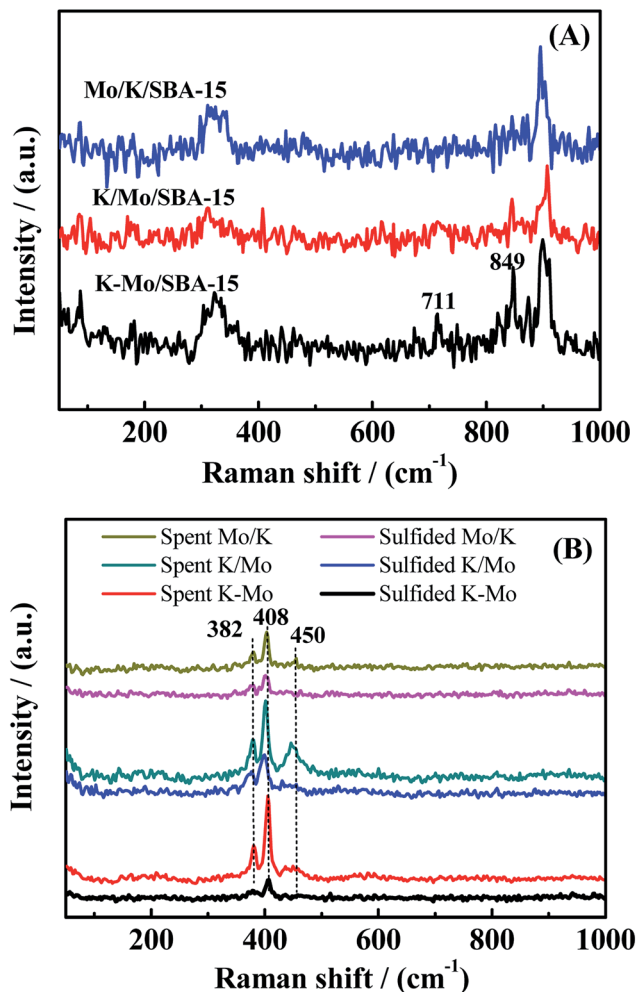


Fig. 3 Raman spectrum of oxide precursor of catalysts (A), sulfided catalysts and spent catalysts (B).

of $\text{Mo}^{\text{IV}}\text{-S}$ for MoS_2 phase, $\text{Mo}^{\text{V}}\text{-O-S}$ surrounded by oxygen and sulfur atoms (intermediate sulfidation phase), $\text{Mo}^{\text{VI}}\text{-O-S}$ species, respectively.³² The spectrum at 226.3, 227.6 and 233.5 eV can be assigned to the S 2s orbit related to S^{2-} (MoS_2), sulfur bridge (S-S^{2-}) and sulfates (SO_4^{2-}), respectively. In the sulfided K-Mo/SBA-15 sample, the relative atomic ratio of $\text{Mo}^{\text{VI}}\text{-S}$, $\text{Mo}^{\text{V}}\text{-O-S}$, $\text{Mo}^{\text{VI}}\text{-O-S}$ (shown in Table 2) is 63.5%, 13.53% and 22.96%, respectively, which indicates that MoS_2 phase is the main species for sulfided sample. After reaction, relative atomic ratio of corresponding species has changed, where the atom% of $\text{Mo}^{\text{VI}}\text{-S}$, $\text{Mo}^{\text{V}}\text{-O-S}$ increases to 71.49% and 13.98% with the decrease of $\text{Mo}^{\text{VI}}\text{-O-S}$ to 14.31%, suggesting the improvement of sulfidation degree when rising the reaction temperature. Those phenomenon are also found in the sulfided Mo/K/SBA-15, K/Mo/SBA-15 samples. Moreover, the binding energy of Mo 3d spectra of spent K-Mo/SBA-15 is slightly higher than that of sulfided sample, which also demonstrates the conversion of partial $\text{Mo}^{\text{VI}}\text{-O-S}$ into $\text{Mo}^{\text{IV}}\text{-S}$ and $\text{Mo}^{\text{V}}\text{-O-S}$ species (higher sulfidation degree). Although there is some transformation in the amount of MoS_2 species between sulfided and spent samples, the selectivity of CH_3SH is not largely changed, suggesting K-Mo/SBA-15 catalyst is relatively stabilized when

sulfided at 553 K. Compared to traditional MoS_2 catalyst that sulfided at higher temperature of 675 K, the sulfidation of K-Mo oxide precursors into surface MoS_2 species at lower temperature of 553 K is enough to convert $\text{CO}/\text{H}_2/\text{H}_2\text{S}$ into CH_3SH . Moreover, the main phase in K/Mo/SBA-15 and Mo/K/SBA-15 obtained through the XPS spectra analysis (presented in Fig. 4C-F) are same with that of K-Mo/SBA-15. The relative atom% of $\text{Mo}^{\text{VI}}\text{-S}$, $\text{Mo}^{\text{V}}\text{-OS}$ and $\text{Mo}^{\text{VI}}\text{-O}$ for K/Mo/SBA-15 and Mo/K/SBA-15 are summarized in Table 2, and the changes in atom% of corresponding phases are followed the rule found in K-Mo/SBA-15. There is very small difference in the $\text{Mo}^{\text{VI}}\text{-S}$ content over K-Mo/SBA-15 and K/Mo/SBA-15 catalysts, while the amount of $\text{Mo}^{\text{VI}}\text{-S}$ in the Mo/K/SBA-15 is largely lower than those of K-Mo/SBA-15 and K/Mo/SBA-15, possibly due to the strong interaction of K with SBA-15 decreasing the sulfidation degree of Mo oxide species.

In general, our goal is to investigate the reaction network for converting $\text{CO}/\text{H}_2/\text{H}_2\text{S}$ to CH_3SH . The difference in the catalytic activity for catalysts prepared by different impregnation sequence is clarified briefly *via* the TPR pattern. As we known, in the typical sulfided MoS_2 based catalysts, sulfur vacancies presented over MoS_2 phases play a significant role in determining the activity of hydrodesulfurization (HDS).^{34,35} Those sulfur vacancy are originated from the removal of sulfur species weakly bonded with molybdenum, which was shown to be labile and was progressively replaced by the sulfur of reactants molecule. Thus, TPR pattern was used to characterize the weakly-bonded and labile surface sulfur species. TPR profiles of three sulfided catalysts are displayed in the Fig. 5. As shown, two kinds of sulfur species are observed in the low and high temperature regions of three catalysts, the low temperature reduction peak between 500–700 K is generally attributed to the reduction of edge reactive sulfur species (*i.e.*, non-stoichiometric, S_x), and the high temperature reduction peak between 800–1000 K corresponds to the recombination of $-\text{SH}$ groups or/and the reduction of K_2S species.^{36,37} The edge reactive sulfur species was generally considered as the active sites and the increase in the peak area at the low-temperature region suggests the growth in the amount of active sites. Generally, the low-temperature peak area for three catalysts is in the following order: Mo/K/SBA-15 < K/Mo/SBA-15 < K-Mo/SBA-15, which is consistent with the catalytic performances for three catalysts (as shown in Fig. 1). Compared the activity results with the TPR results, CO conversions of Mo/K/SBA-15, K/Mo/SBA-15, K-Mo/SBA-15 catalysts were correlated to the number of edge reactive sulfur species to some degree.

The reaction pathway for synthesizing CH_3SH with $\text{CO}/\text{H}_2\text{S}/\text{H}_2$

It is well known that carbonyl sulfide (COS) is one of significant intermediates in the synthesis of CH_3SH with $\text{CO}/\text{H}_2\text{S}/\text{H}_2$,^{16,38} thus indicating that COS might be dominantly presented in the products and the selectivity of COS could increase with the increasing conversion of CO, as depicted with the reaction eqn (2) However, a diametrically drop in the COS selectivity was observed at our experiment conditions (Fig. 1). The above phenomena can be interpreted as follows: the downward trend



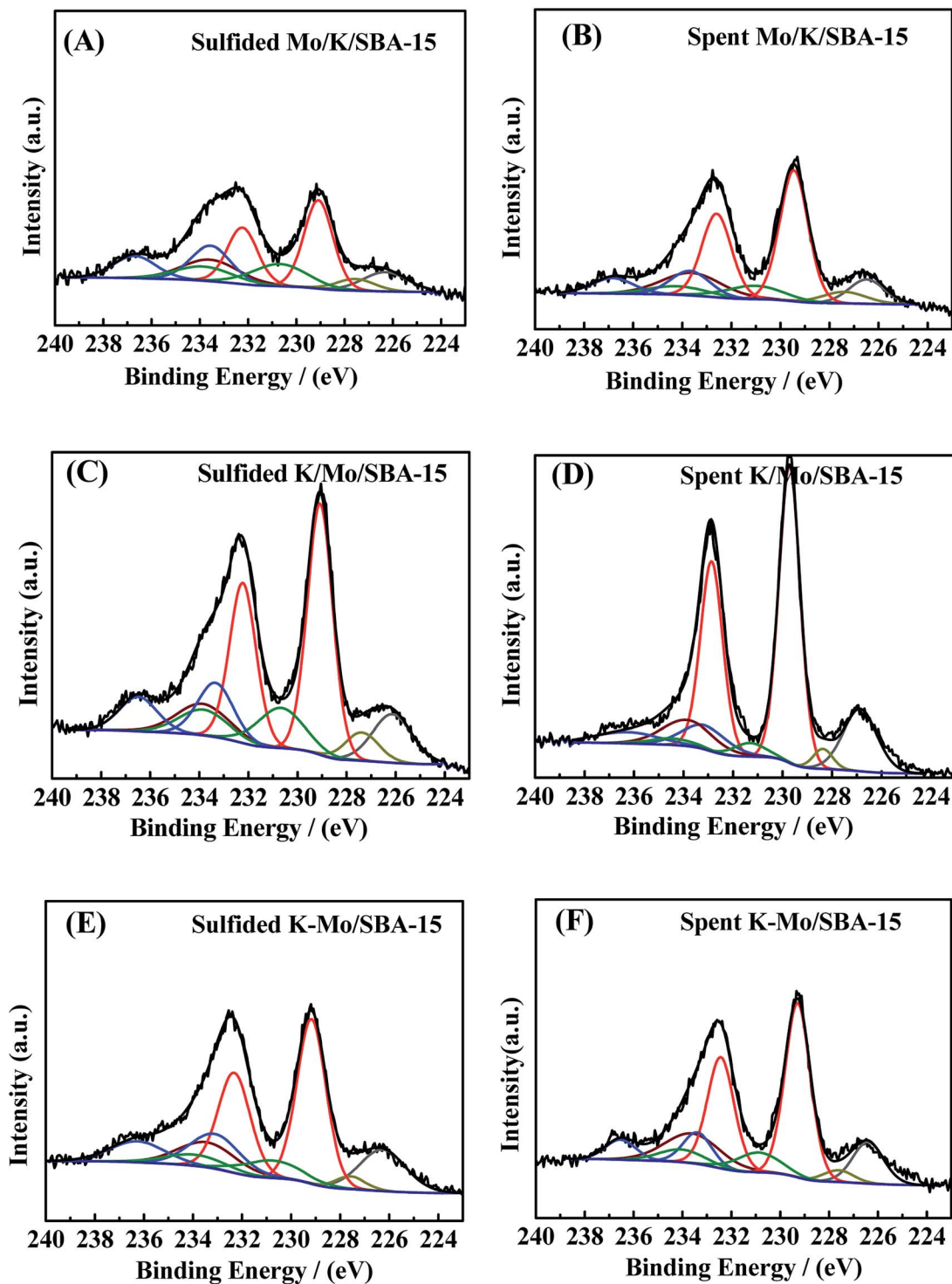


Fig. 4 XPS spectra of the Mo 3d–S 2s core level of (A) sulfided Mo/K/SBA-15, (B) spent Mo/K/SBA-15, (C) sulfided K/Mo/SBA-15, (D) spent K/Mo/SBA-15 (E) sulfided K–Mo/SBA-15, and (F) spent K–Mo/SBA-15.

of COS selectivity as temperature rising indicates that the reaction rate for consuming COS was faster than that for producing COS *via* eqn (2); the low COS selectivity reveals that the large portion of COS generated from eqn (2) should be rapidly consumed *via* some reaction pathways as depicted by eqn (3)–(6). In all four reactions, it seems to consider that the reaction for consuming COS by eqn (5) rarely generate due to

the presence of reverse reaction of (2). The reaction (6) should be occurred owing to the generation of CO₂ in our reaction system. If the presence of reactions (3) and (4) or not can be confirmed by the formed CH₃SH. As can be seen from Fig. 1, the increasing in the selectivity of CH₃SH until reaching a maximum at 573 K with the increase of reaction temperature was accompanied by the decrease in the selectivity of COS,

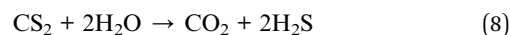
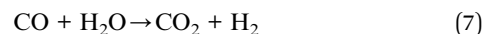
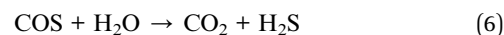
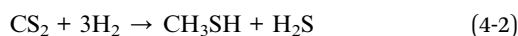
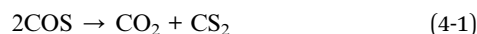
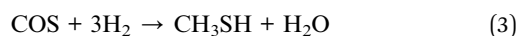


Table 2 Relative atom% of Mo species in sulfided and spent catalysts

Catalyst	Sulfided catalysts			Spent catalysts		
	Mo ^{VI} -S ^a (%)	Mo ^V -OS ^b (%)	Mo ^{VI} -O ^c (%)	Mo ^{VI} -S (%)	Mo ^V -OS (%)	Mo ^{VI} -O (%)
Mo/K/SBA-15	49.1	23.66	25.84	68.29	14.00	16.25
K/Mo/SBA-15	62.61	18.29	18.80	79.37	5.44	11.97
K-Mo/SBA-15	63.50	13.53	22.96	71.49	13.98	14.31

^a The Mo^{IV} species related to MoS₂. ^b The Mo^V surrounded by oxygen and sulfur atoms. ^c The oxidized Mo^{VI} species.

which is attributed to the conversion of COS to form CH₃SH. Notably, the generation of CH₃SH can be responsible for the only two independent reaction pathways by means of eqn (3) or (4) which could occur under different amount of COS and have been proposed by many groups, respectively.^{16,19,22,23} As for the former reaction pathway, some of the early reports^{16,19} had been considered the hydrogenation of COS to generate CH₃SH and H₂O to be the sole source of CH₃SH formation, and COS was the only intermediate species in this synthetic reaction. With respect to the latter reaction pathway, it had been proposed by Lercher and coworkers in the recent study,^{22,23,39} and they pointed out that eqn (4) was composed of two step reactions: the first step was the disproportionation of COS to produce carbon dioxide (CO₂) and carbon disulfide (CS₂) (eqn (4-1)); the second step was the hydrogenation of CS₂ to form CH₃SH (eqn (4-2)).



In light of the above fact, two reaction pathways were possibly presented. However, to our best knowledge, at present, no evidence was provided to prove the coexistence of those two reactions pathways. It should be stated that the conversion of mixed CO/H₂S/H₂ into CH₃SH is rather complex because there are more than ten matters (CO, H₂S, H₂, COS, CH₃SH, CO₂, CS₂, CH₄, C₂H₄, C₂H₆, CH₃SCH₃, CH₃SSCH₃, shown in Fig. 1-S of ESI†) and more than ten reactions (eqn (1) to (12)) presented in the reaction system. Employing three starting reactants (CO/H₂S/H₂ or COS/H₂S/H₂ or CS₂/H₂S/H₂) as a whole or system is difficult to completely understand the reaction pathways for the conversion of mixed CO/H₂S/H₂ into CH₃SH due to its complexity, as previously reported in the literature.^{19,22,40} The separation of integral three starting reactants into individual two reactants may provide a new view to investigate the complex reaction process. Based on our analysis, the production of water is a key point to prove the existence of former reaction pathway in our synthetic reaction. In our work, large amount of water peak can be found in TCD with a PQ volume when using synthetic gas (CO/H₂/H₂S = 1 : 5 : 4) to synthesize CH₃SH over three catalysts (shown in Fig. 3-S of ESI†), thus it is necessary to investigate if there are some other reactions that can generate water. Totally, four reactions in our reaction system possibly produce H₂O as listed in the follows: COS + 3H₂ → CH₃SH + H₂O (eqn (3)); CO₂ + H₂S → COS + H₂O (the reverse reaction of eqn (6)); CO₂ + H₂ → CO + H₂O (the reverse reaction of eqn (8)); CO + 3H₂ → CH₄ + H₂O (eqn (7)). K-Mo/SBA-15 was selected to investigate the catalytic performance of above-mentioned reactions in the following. For the reverse reaction of eqn (6), the usage of CO₂ : H₂S : N₂ = 1 : 1 : 8 (30 ml min⁻¹) as reactants was investigated and the result is presented in Fig. 6A. It is seen that the conversion of CO₂ is pretty low (2–4%) and there is also no water peak found in TCD (shown in Fig. 2-S(A) of ESI†), indicating that large amount of water is not possibly produced from eqn (6). For the reverse reaction of eqn (8), CO₂ : H₂ : N₂ = 1 : 1 : 8 (30 ml min⁻¹) was used to research the reaction completion degree and the result is shown in Fig. 6B. The conversion of CO₂ is rising with the temperature increasing and reaches the maximal value at 673 K, while only 13.46% CO₂ was converted, more importantly, the peak of water cannot be found in

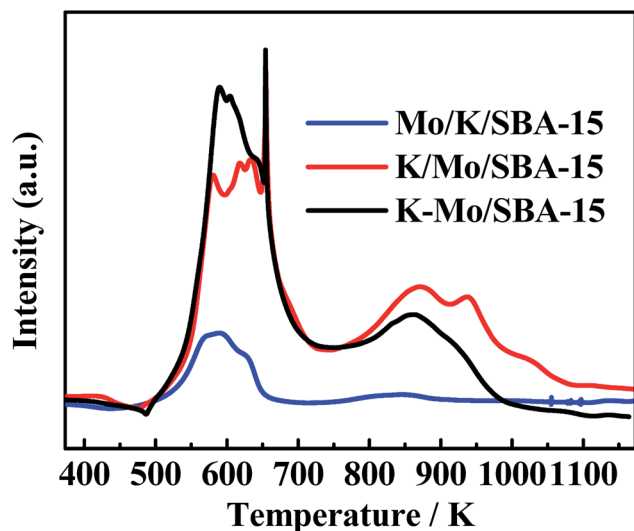


Fig. 5 TPR patterns of sulfided Mo/K/SBA-15, K/Mo/SBA-15 and K-Mo/SBA-15.



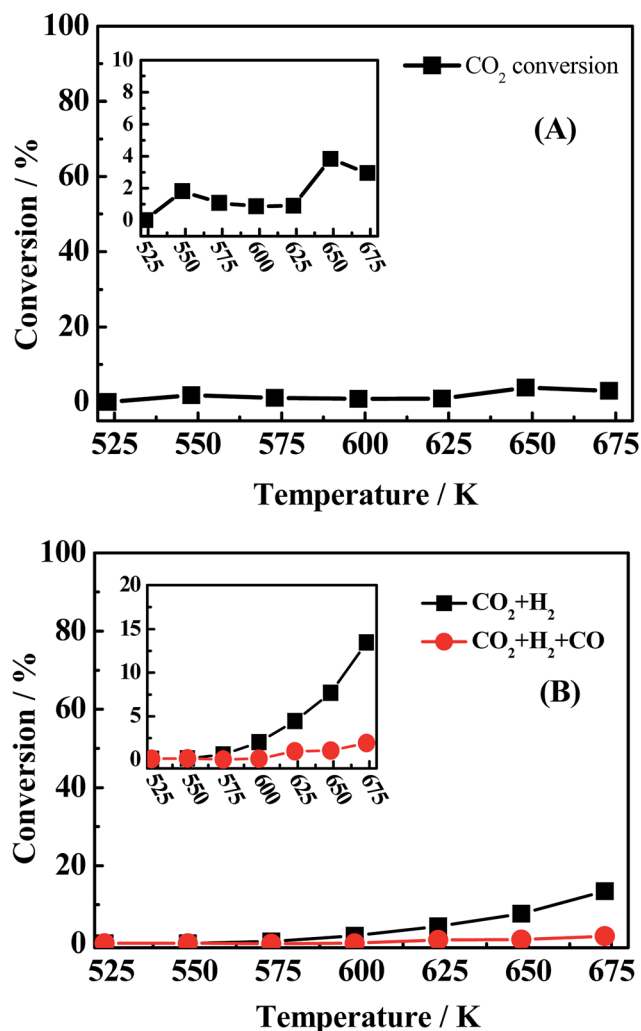


Fig. 6 CO conversion (black light square) of (A) reaction conditions: 0.2 MPa, 1000 h⁻¹ and CO₂/H₂S/N₂ = 1 : 1 : 8 (30 ml min⁻¹), (B) reaction conditions: 0.2 MPa, 1000 h⁻¹, CO₂/H₂/N₂ = 1 : 1 : 8 (30 ml min⁻¹) and CO₂/H₂/CO/N₂ = 1 : 1 : 1 : 7 (30 ml min⁻¹).

the TCD (shown in Fig. 2-S(B) of ESI[†]). Actually, this reverse water gas shift reaction is hardly to occur in this condition due to the high concentration of CO atmosphere in the system, the water gas shift reaction is more likely to happen under that condition. The sequence experiment of the reverse water gas shift reaction with adding 10% CO (v/v) also confirms our view. As for eqn (7), using CO/H₂ = 1 : 4 (30 ml min⁻¹) as the reactant gas was investigated and the result is shown in Fig. 7. It can be found that the CO conversion is pretty low and the main product is CH₄ and CO₂ with a little C₂H₄ and C₂H₆, this indicating the generation of CH₄ from CO with H₂ (2CO + 2H₂ → CH₄ + CO₂)⁴¹ instead of the reaction (CO + 3H₂ → CH₄ + H₂O). Accordingly, large amount of water in system is produced from the hydrogenation of COS (eqn (3)) which indicates the first reaction pathway would happen certainly.

In order to have a further acquaintance to the whole reaction pathway, another two reactions using different components as reactant gas were investigated and compared. The activity experimental result of the reaction using CO/H₂S = 1 : 5 as reactant gas (denote as R(CO/H₂S)) was shown in Fig. 8(A) and

used to compare with the reaction using CO/H₂S/H₂ as reactant gas in Fig. 8(B) (denote as R(CO/H₂S/H₂)). The only difference between R(CO/H₂S/H₂) and R(CO/H₂S) is the concentration of H₂ in reaction system. The amount of hydrogen in the first reaction is sufficient but it is shortage in the second reaction because H₂ in the system of R(CO/H₂S) can be generated from eqn (2). In R(CO/H₂S) system, the selectivities of two main species COS and CS₂ are found to be 33–32% and 6–15% from 523 K to 675 K, respectively. The presence of large amount of CS₂ in R(CO/H₂S) system indicates that CS₂ is the significant intermediate species and the disproportionation of COS (eqn (4-1)) occurs indeed. In R(CO/H₂S/H₂) system, however, it is found that the corresponding selectivities of two species decrease largely (16–8% and 0–1.4% from 523 K to 675 K, respectively). It suggests that the addition of hydrogen leads to the large consumption of COS and CS₂, indicating the hydrogenation of CS₂ has happened as eqn (4-2). In basis of the above facts, we proposed that two reaction pathways may be occurred simultaneously in our reaction system. Comparison of the selectivity of CO₂ between R(CO/H₂S/H₂) and R(CO/H₂S) also demonstrates this point. The corresponding result is displayed in Fig. 8(C). As we known, if only the former reaction pathway, *i.e.*, the hydrogenation of COS accompanied by reaction of COS and H₂O to generate CO₂, exists, the amount of CO₂ in H₂-rich system (R(CO/H₂S/H₂)) would be lower than that in H₂-deficient system (R(CO/H₂S)) because more H₂ was added and then more COS was consumed to generate CH₃SH, instead of CO₂. While if only the latter reaction pathway, *i.e.*, the disproportionation of COS followed by the hydrogenation of CS₂, is presented, the amount of CO₂ in H₂-rich system (R(CO/H₂S/H₂)) would be higher than that in H₂-deficient system (R(CO/H₂S)) because more H₂ was added and then more CS₂ was consumed, leading to a big surplus of CO₂. However, in our work, the selectivity of CO₂ between R(CO/H₂S/H₂) and R(CO/H₂S) exhibits interlaced results at all the reaction temperature range (Fig. 8C), which confirms the coexistence of two reaction pathways. Moreover, large amount of by-product CO₂ is found to be presented in the products and is almost stabilized at all the reaction temperature

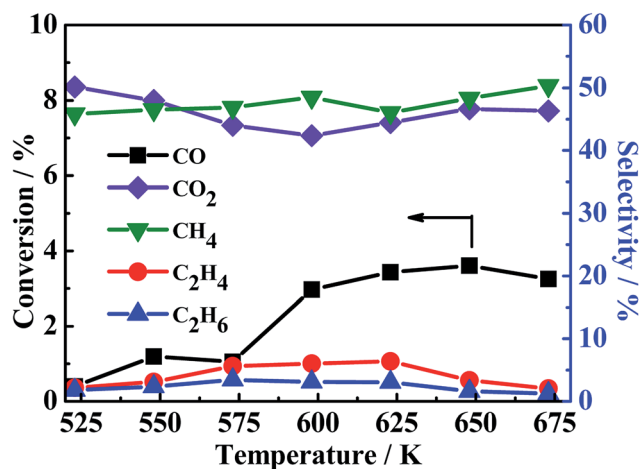


Fig. 7 CO conversion (black light square) and CH₄ (green light square), C₂H₄ (red light ball) and C₂H₆ (blue light triangle) selectivity. Reaction conditions: 0.2 MPa, 1000 h⁻¹ and CO/H₂ = 1 : 4 (30 ml min⁻¹).



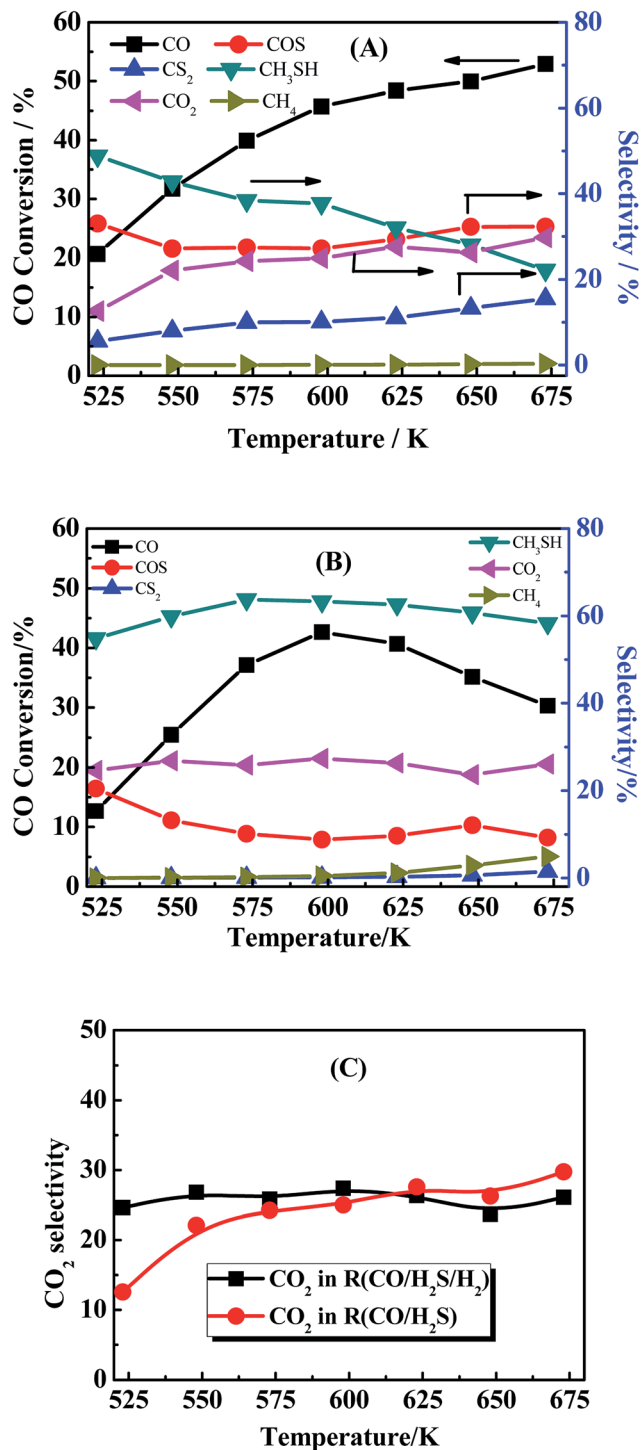


Fig. 8 (A) CO conversion (black square light) and the product selectivity (marked in the picture). Reaction conditions: 0.2 MPa, 1000 h⁻¹ and CO/H₂S = 1 : 5 (30 ml min⁻¹). (B) CO conversion (black square light) and the product selectivity (marked in the picture). Reaction conditions: 0.2 MPa, 1000 h⁻¹ and CO/H₂S/H₂ = 1 : 5 : 4 (30 ml min⁻¹). (C) Comparison of CO₂ selectivity between in R(CO/H₂S/H₂) and R(CO/H₂S).

region. This generated CO₂ is mainly derived from the disproportionation of COS from eqn (4-1) and the hydrolysis of COS, CO, CS₂ from eqn (6)–(8) respectively.

Another phenomenon should be taken into consideration. In the theoretical point, when CO conversion is increasing with the temperature rising, the amount of generated H₂ should be increasing, and CS₂ and COS can be easily reacted with generated H₂ to generate more CH₃SH (eqn (4-2)). However, it is noted that the selectivity of CH₃SH in R(CO/H₂S) sharply decreases with the increasing temperature. Two reasons could be responsible for this phenomenon. On the one hand, the decreasing in the CH₃SH selectivity may be partially due to the reduction in the generation of CH₃SH, which is proved by the increased selectivity of CS₂. On the another hand, CH₃SH could be decomposed all the time to other matters. The low selectivity of CH₄ in R(CO/H₂S) system indicates the large decrease in the CH₃SH selectivity may be not completely originated from the decomposition of CH₃SH into CH₄, and may be attributed to the decomposition of CH₃SH into other matters under hydrogen shortage atmosphere. To confirm the view we proposed, the experiment using CH₃SH as reactant gas was carried out, and the CH₃SH conversion and product selectivity are presented in Fig. 9. We are surprised to find that the conversion of CH₃SH is pretty high and has arrived 97% at 623 K, the main components in relatively lower temperature are dimethyl sulfide (CH₃SCH₃) and dimethyl disulfide (CH₃SSCH₃), and those products are decreasing with the temperature increasing and CH₄ becomes the predominant product when the temperature is more than 593 K. Those result indicate that the conversion of CH₃SH was firstly converted into intermediates, CH₃SCH₃ and CH₃SSCH₃, and then the intermediates were decomposed into CH₄ and H₂S, as described in eqn ((9-1)–(9-4)). However, the low and unchanged selectivity of CH₄ in R(CO/H₂S) system can not explain the drastic decrease in the CH₃SH selectivity and some other reason should be presented. The spent catalyst was characterized by Raman spectrum to detect if the carbon deposition was presented and the result is shown in Fig. 10. It is obvious that the catalyst for R(CH₃SH) exhibits a Raman band between 1300–1700 cm⁻¹ which is attributed to carbon deposition,^{42,43} indicating that CH₃SH could be possibly decomposed

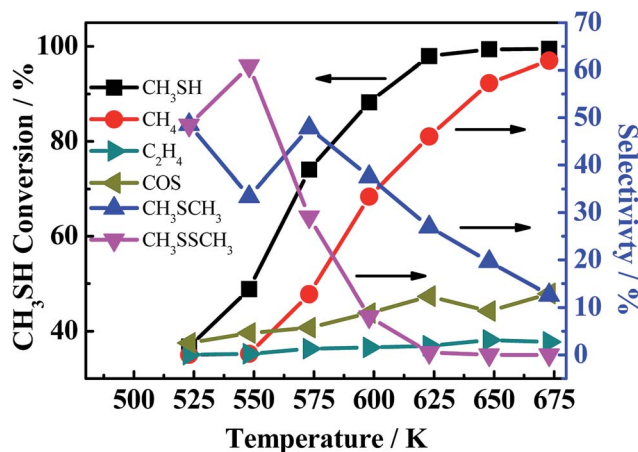
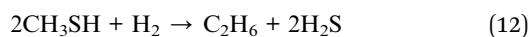
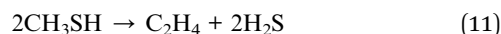
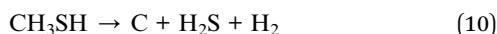
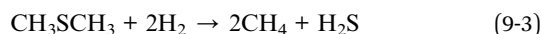
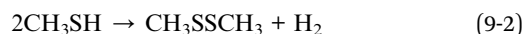
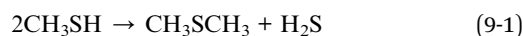
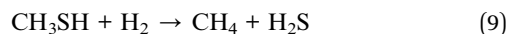


Fig. 9 CH₃SH conversion (black light square) and the product selectivity (marked in the picture). Reaction conditions: 0.2 MPa, 1000 h⁻¹, 30 ml min⁻¹.



to H₂S, H₂ and C, as shown by eqn (10). Certainly, some other possible reason for the decreased selectivity of CH₃SH can not be excluded. Moreover, due to the monitoring of trace amounts of ethylene (C₂H₄) and ethane (C₂H₆), the reactions (11) and (12) would be occurred to some degree in the reaction system.



Thus, we considered that CH₃SH in the reaction system is in a state of equilibrium of generation and decomposition. Therefore, it is concluded that the general reaction pathways are according to the following routes, as illustrated and described in Fig. 11.

Thermodynamics study

Due to the fact that the thermodynamic analysis is an important criterion for the possibility and the degree of a chemical reaction, the feasibility of some important intermediate process involved in our reaction system was further demonstrated and discussed by using the results of thermodynamic calculation. Thermodynamic data (the changes of Gibbs free energy and enthalpy, equilibrium constant) of CH₃SH-free reactions were determined by using HSC Chemistry 5.1 software, however, as

a result of the lack of the fundamental parameter about CH₃SH in the HSC software, the corresponding thermodynamics data of CH₃SH-containing reactions were calculated by the Kirchhoff Law⁴⁴ and the modified Gibbs–Helmholtz equation.^{45,46} The fundamental thermodynamic parameter of partial substances for reactions containing CH₃SH are compiled in the Table 1-S (shown in the ESI†). The considerable of these calculation formulas as a feasible method could be ascribed to the fact that each reaction was performed under the condition of constant low pressure (0.2 MPa) and constant high temperature (≥548 K), which could be deemed to be the ideal gas and satisfied the applicable conditions of above equations.

The thermodynamic data of all the reactions were calculated and summarized in the Tables 2-S and 3-S in the ESI.† Gibbs free energy change and equilibrium constant of main reactions to produce CH₃SH and CO₂ are displayed in Fig. 12 and 13, respectively. Two reactions involving the hydrogenation of COS to produce CH₃SH (eqn (3) and (4)) should be firstly taken into account owing to the uncertainty whether these two reactions could automatically occur and which reaction is predominant. It can be observed from Table 2-S† that two reactions related to the formation of CH₃SH at the temperature range of 548 K to 648 K are exothermic. From the thermodynamic point of view, it seems to be indicated that the increase of reaction temperature would facilitate the process of reactions (3) and (4). In combination with the changes of Gibbs free energy and equilibrium constant from Fig. 12 and Table 2-S,† it could be concluded that both the reactions (3) and (4) might occur spontaneously in thermodynamics ($\Delta G_r(T) < 0$). This further confirms our experimental results that the reaction (3) and (4) should be presented simultaneously in the reaction system. Moreover, the thermodynamic equilibrium constant of reaction (4) ($= 1.19 \times 10^4$ at 573 K) is about three order greater in magnitude than that of the reaction (3) ($= 23.77$ at 573 K). This result signifies that, in thermodynamics, reaction (4) might easily occur than the reaction (3).

Another several uncertain side pathways are the reactions to form by-products CO₂ by the hydrolysis of COS, CO and CS₂ *via* the reactions of (6)–(8), respectively. The thermodynamic data are shown in Fig. 13 and Table 3-S(A).† As seen from the results, all the hydrolysis reactions are deemed to be exothermic and could occur spontaneously. Among them, the equilibrium constant of the hydrolysis reaction of CS₂ ($K_p \approx 10^6$) is the maximum, suggesting that it is more likely to occur than the other two reactions in thermodynamics. As the reaction temperature increasing, the equilibrium constant of hydrolysis reaction of CS₂ keeps the same order of magnitude. Therefore, it seems to be considered that the impact of temperature on this reaction turns out to be very small. However, the influence of temperature on thermodynamic equilibrium constant for the hydrogenation of CS₂ is relative larger than that of the hydrolysis of CS₂, which suggests that increasing reaction temperature do not facilitate the hydrogenation of CS₂. In order to further corroborate the accuracy of the method calculated by thermodynamic equations on the CH₃SH-containing reactions, the thermodynamic data of three hydrolysis reactions are both calculated by the thermodynamic equations and HSC software,

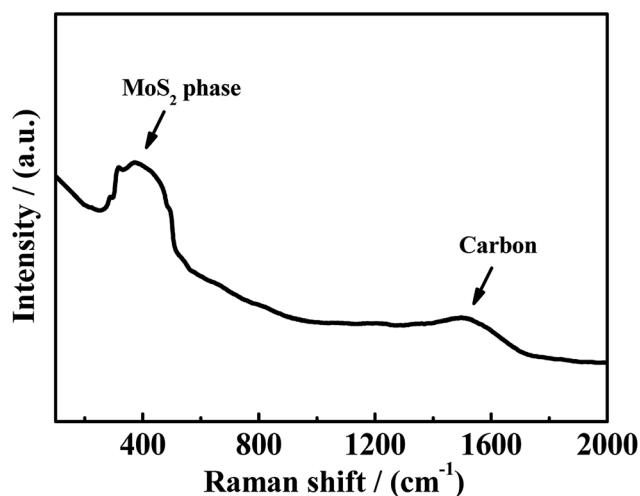


Fig. 10 Raman spectrum of spent catalysts in R(CH₃SH).



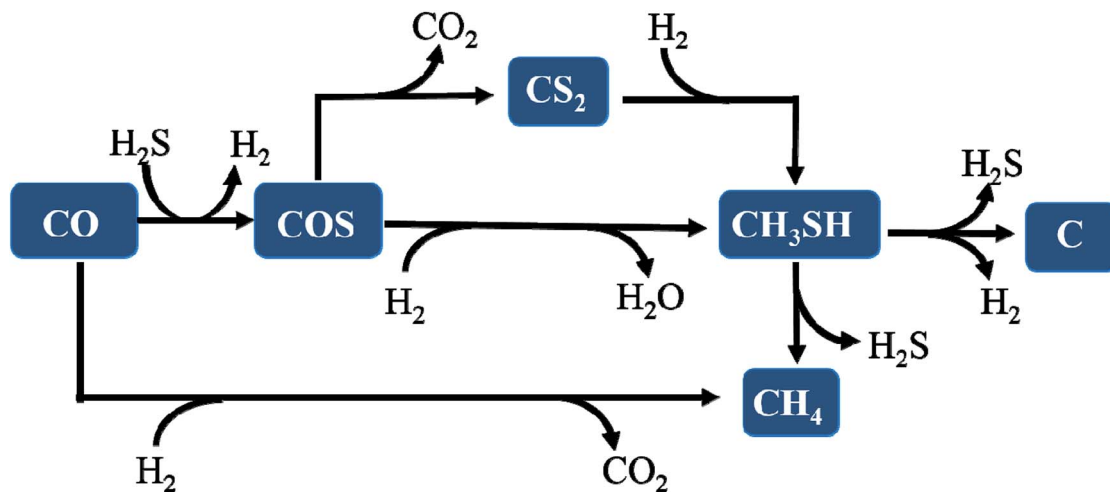


Fig. 11 The reaction pathway for synthesizing CH_3SH from $\text{CO}/\text{H}_2\text{S}/\text{H}_2$ gas.

and the corresponding results are tabulated in Table 3-S(B).[†] It can be observed that the reaction enthalpy change, Gibbs free energy change and equilibrium constant of these reactions calculated by thermodynamic equations are in good agreement with HSC software.

The corresponding catalytic reaction mechanism for the conversion of $\text{CO}/\text{H}_2/\text{H}_2\text{S}$ to CH_3SH over SBA-15 supported K–Mo catalysts are clarified briefly. In general, in the conversion of $\text{CO}/\text{H}_2/\text{H}_2\text{S}$ to CH_3SH , CO was firstly reacted with H_2S to produce COS, and subsequently, the direct or indirect hydrogenation of COS results in the generation of CH_3SH . In our previous work, sulfided MoS_2 catalyst without the addition of K species was demonstrated to have no ability to produce CH_3SH , while the incorporation of K species into MoS_2 species

gives rise to the significant generation of CH_3SH .²⁶ Thus, the synergistic interaction between K and MoS_2 species is crucial to the generation of CH_3SH . It is known that the sulfur vacancies over MoS_2 phases derived from the removal of sulfur species weakly bonded with molybdenum in the reaction process can activate the reactant molecules of CO, H_2 , H_2S and were the reactive active sites. In our reaction system ($\text{CO}/\text{H}_2/\text{H}_2\text{S}$), CO and H_2S molecules were thus non-dissociatively and dissociatively absorbed on the sulfur vacancies, respectively, to generate the intermediate, COS. With the activation of H_2 molecule over the sulfur vacancies, the further direct or indirect hydrogenation of COS leads to the formation of CH_3SH via stabilizing C–S bond by K species.^{22,23}

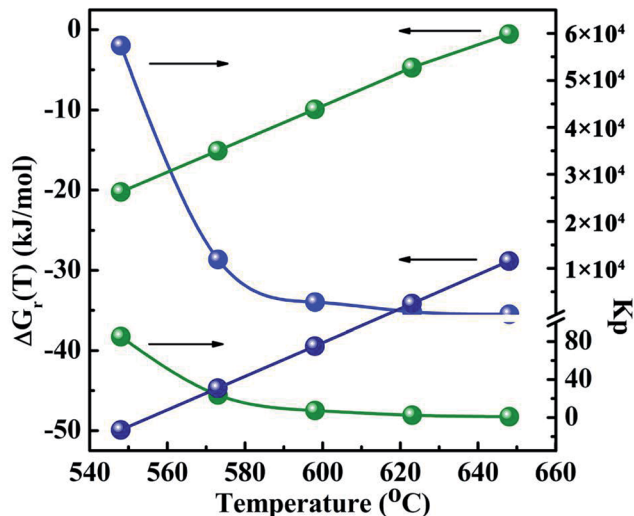


Fig. 12 The Gibbs free energy changes and thermodynamic equilibrium constants of main reactions as a function of temperature. The blue light ball: $\text{COS} + 3\text{H}_2 \rightarrow \text{CH}_3\text{SH} + \text{H}_2\text{O}$ eqn (3); the green light ball: $2\text{COS} + 3\text{H}_2 \rightarrow \text{CH}_3\text{SH} + \text{CO}_2 + \text{H}_2\text{S}$ eqn (4).

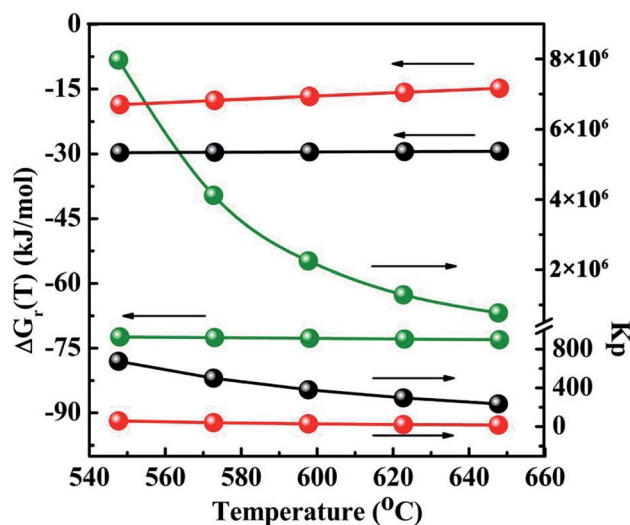


Fig. 13 The Gibbs free energy changes and thermodynamic equilibrium constants of side reactions as a function of temperature. The black light ball: $\text{COS} + \text{H}_2\text{O} \rightarrow \text{CO}_2 + \text{H}_2\text{S}$ eqn (6); the red light ball: $\text{CO} + \text{H}_2\text{O} \rightarrow \text{CO}_2 + \text{H}_2$, eqn (7); the green light ball: $\text{CS}_2 + 2\text{H}_2\text{O} \rightarrow \text{CO}_2 + 2\text{H}_2\text{S}$ eqn (8).



Conclusion

The influences of the impregnation sequence on the conversion of CO and the selectivity of CH₃SH, COS, CO₂ and CH₄ over SBA-15 supported Mo based catalysts were investigated and compared. The catalytic performances of catalysts are in the order of K–Mo/SBA-15 > K/Mo/SBA-15 > Mo/K/SBA-15. Based on the characterizations results, two K-containing Mo oxides (K₂Mo₂O₇ and K₂MoO₄) were detected as main species in the oxidized samples, and amorphous MoS₂ is predominated in the corresponding sulfided and spent samples. The CO conversion was closely related to the amount of the edge reactive sulfur species that formed the sulfur vacancies over MoS₂ phases. Combining experimental data with the results of thermodynamics analyses, the corresponding reaction pathways over K–Mo/SBA-15 were proposed. CO was firstly reacted with H₂S to produce COS, and CH₃SH was formed *via* two reaction pathways: the first one is the direct hydrogenation of COS, and the second one is the hydrogenation of CS₂ originated from the disproportionation of COS. CH₃SH in reaction system is in a state of equilibrium of generation and decomposition, the selectivity of CH₃SH would decrease with the temperature increasing due to the enhancement of decomposition reaction and thermodynamic limit. Two reaction pathways were found to result in the decomposition of CH₃SH, on the one hand, CH₃SH is firstly converted into intermediates, CH₃SCH₃ and CH₃SSCH₃, and then those species can be decomposed into CH₄ and H₂S. On the other hand, some CH₃SH could probably decompose to carbon, H₂S and H₂.

Conflicts of interest

There are no conflicts to declare.

Acknowledgements

We gratefully acknowledge the financial support of the research work from the National Natural Science Foundation of China (Grant No. 21367015, 21267011, 21667016 and U1402233), and Young Academic and Technical Leader Raising Foundation of Yunnan Province (Grant No. 2008py010).

References

- 1 Y. Z. Li, H. L. Tong, Y. Q. Zhuo, S. J. Wang and X. C. Xu, *Environ. Sci. Technol.*, 2010, **40**, 7919–7924.
- 2 Z. Zhang, Y. Zhu, H. Asakura, B. Zhang, J. Zhang, M. Zhou, Y. Han, T. Tanaka, A. Wang, T. Zhang and N. Yan, *Nat. Commun.*, 2017, **8**, 16100.
- 3 J. G. Lu, Y. F. Zheng and D. L. He, *Sep. Purif. Technol.*, 2006, **52**, 209–217.
- 4 D. K. Chen, D. D. He, J. C. Lu, L. P. Zhong, F. Liu, J. P. Liu, J. Yu, G. P. Wan, S. F. He and Y. M. Luo, *Appl. Catal., B*, 2017, **218**, 249–259.
- 5 V. P. Santos, B. V. D. Linden, A. Chojecki, G. Budroni, S. Corthals, H. Shibata, G. R. Meima, F. Kapteijn, M. Makkee and J. Gascon, *ACS Catal.*, 2013, **3**, 1634–1637.
- 6 R. Andersson, M. Boutonnet and S. Järås, *Fuel*, 2014, **115**, 544–550.
- 7 Y. Q. Yang, Y. Z. Yuan, S. J. Dai, B. Wang and H. B. Zhan, *Catal. Lett.*, 1998, **54**, 65–68.
- 8 J. Olin, B. Buchholz, B. Love, R. Goshorn, U.S. Patent No. 3070632. 1962.
- 9 Y. Zhang, S. Chen, M. Wu, W. P. Fang and Y. Q. Yang, *Catal. Commun.*, 2012, **22**, 48–51.
- 10 T. J. Paskach, G. L. Schrader and R. E. McCarley, *J. Catal.*, 2002, **211**, 285–295.
- 11 J. Sauer, W. Boeck, L. V. Hippel, W. Burkhardt, S. Rautenberg, D. Arntz, W. Hofen, *US. Pat. No.* 5852219. 1998.
- 12 V. Mashkin, V. Kudenkov and A. V. Mashkina, *Ind. Eng. Chem. Res.*, 1995, **34**, 2964–2970.
- 13 J. C. Lu, X. F. Li, S. F. He, C. Y. Han, G. P. Wan, Y. Q. Lei, R. Chen, P. Liu, K. Z. Chen, L. Zhang and Y. M. Luo, *Int. J. Hydrogen Energy*, 2017, **42**, 3647–3657.
- 14 Y. Q. Yang, Y. J. Hao, A. P. Chen, Q. Wang, L. M. Yang, Q. L. Li, S. J. Dai, W. P. Fang, J. O. Barth, C. Webecker, K. Huttmacher, *US. Pat. No.* 0286448 A1. 2010.
- 15 Y. Q. Yang, H. Yang, Q. Wang, L. J. Yu, C. Wang, S. J. Dai and Y. Z. Yuan, *Catal. Lett.*, 2001, **74**, 221–225.
- 16 A. P. Chen, Q. Wang, Y. J. Hao, W. P. Fang and Y. Q. Yang, *Catal. Lett.*, 2008, **121**, 260–265.
- 17 S. J. Dai, Y. Q. Yang, Y. Z. Yuan, D. L. Tang, R. C. Lin and H. B. Zhang, *Catal. Lett.*, 1999, **61**, 157–160.
- 18 Y. Q. Yang, S. J. Dai, Y. Z. Yuan, R. C. Lin, D. L. Tang and H. B. Zhang, *Appl. Catal., A*, 2000, **192**, 175–180.
- 19 J. Barrault, M. Boulinguez, C. Forquy and R. Maurel, *Appl. Catal.*, 1987, **33**, 309–330.
- 20 B. J. Zhang, S. H. Taylor and G. J. Hutchings, *New J. Chem.*, 2004, **28**, 471–476.
- 21 W. Cao, H. Zhang and Y. Yuan, *Catal. Lett.*, 2003, **91**, 243–246.
- 22 O. Y. Gutiérrez, C. Kaufmann, A. Hrabar, Y. Z. Zhu and J. A. Lercher, *J. Catal.*, 2011, **280**, 264–273.
- 23 O. Y. Gutiérrez, C. Kaufmann and J. A. Lercher, *ACS Catal.*, 2011, **1**, 1595–1603.
- 24 S. Y. He, S. F. He, L. Zhang, X. F. Li, J. Wang, D. D. He, J. C. Lu and Y. M. Luo, *Catal. Today*, 2015, **258**, 162–168.
- 25 H. P. Pu, C. Y. Han, H. Wang, S. W. Xu, L. Y. Zhang, Y. Y. Zhang and Y. M. Luo, *Appl. Surf. Sci.*, 2012, **258**, 8895–8901.
- 26 P. Liu, J. C. Lu, Z. Z. Xu, F. Liu, D. K. Chen, J. Yu, J. P. Liu, S. F. He, G. P. Wan and Y. M. Luo, *Mol. Catal.*, 2017, **442**, 39–48.
- 27 S. Huang, S. F. He, L. Deng, J. Wang, D. D. He, J. C. Lu and Y. M. Luo, *Procedia Eng.*, 2015, **102**, 684–691.
- 28 Y. M. Luo, Z. Y. Hou, R. T. Li and X. M. Zheng, *Microporous Mesoporous Mater.*, 2008, **109**, 583–589.
- 29 Q. Liu, Y. Qiao, Y. Tian, F. Gu, Z. Zhong and F. Su, *Ind. Eng. Chem. Res.*, 2017, **56**, 9809–9820.
- 30 V. Kettmann, P. Balgavy and L. Sokol, *J. Catal.*, 1988, **112**, 93–106.
- 31 G. Schrader and C. Cheng, *J. Catal.*, 1983, **80**, 369–385.



- 32 A. Cordova, P. Blanchard and C. Lancelot, *ACS Catal.*, 2015, **5**, 2966–2981.
- 33 L. Qiu and G. Xu, *Appl. Surf. Sci.*, 2010, **256**, 3413–3417.
- 34 B. M. Vogelaar, P. Steiner, T. F. Zijden, A. D. Langeveld, S. Eijsbouts and J. A. Moulijn, *Appl. Catal., A*, 2007, **318**, 28–36.
- 35 L. S. Byskov, B. Hammer, J. K. Norskov, B. S. Clausen and H. Topsøe, *Catal. Lett.*, 1997, **47**, 177–182.
- 36 E. P. Polo, A. G. Alejandre, G. González and J. L. Brito, *Catal. Lett.*, 2010, **135**, 212–218.
- 37 D. Ishutenko, P. Minaev, Y. Anashkin, M. Nikulshina, A. Mozhaev, K. Maslakov and P. Nikulshin, *Appl. Catal., B*, 2017, **203**, 237–246.
- 38 G. Mul, I. E. Wachs and A. S. Hirschon, *Catal. Today*, 2003, **78**, 327–337.
- 39 O. Y. Gutiérrez, C. Kaufmann and J. A. Lercher, *ChemCatChem*, 2011, **3**, 1480–1490.
- 40 O. Y. Gutiérrez, L. S. Zhong, Y. Z. Zhu and J. A. Lercher, *ChemCatChem*, 2013, **5**, 3249–3259.
- 41 Q. Liu, Y. Tianab and H. Ai, *RSC Adv.*, 2016, **6**, 20971.
- 42 A. C. Ferrari and J. Robertson, *Phys. Rev. B*, 2000, **61**, 14095.
- 43 J. C. Lu, H. S. Hao, L. M. Zhang, Z. Z. Xu, L. P. Zhong, Y. T. Zhao, D. D. He, J. P. Liu, D. K. Chen, H. P. Pu, S. F. He and Y. M. Luo, *Appl. Catal., B*, 2018, **237**, 185–197.
- 44 J. W. Tester and M. Modell, *Thermodynamics and its Applications*, Prentice Hall PTR, 1997.
- 45 B. E. Poling, J. M. Prausnitz and J. P. Oconnell, *The properties of gases and liquids*, New York: Mcgraw-hill, 2001.
- 46 D. R. Lide, J. Shackleton, T. Desai, N. Kamaly, M. Griffiths and L. Braschi, *CRC Handbook of Chemical and Physics*, 84th edn, 2003–2004.

